AECD-2706

UNITED STATES ATOMIC ENERGY COMMISSION

RELATIVE PHOTOFISSION CROSS SECTIONS OF SEVERAL FISSIONABLE MATERIALS

by

John McElhinney
William Ogle

Los Alamos Scientific Laboratory

This document is reproduced as a project report and is without editorial preparation. The manuscript has been submitted to The Physical Review for possible publication.

Date of Manuscript: February 18, 1949
Date Declassified: September 13, 1949

Technical Information Division, ORE, Oak Ridge, Tennessee
AEC, Oak Ridge, Tenn., 2-10-50--850-A14034

PRINTED IN USA
PRICE 10 CENTS

DISCLAIMER NOTICE

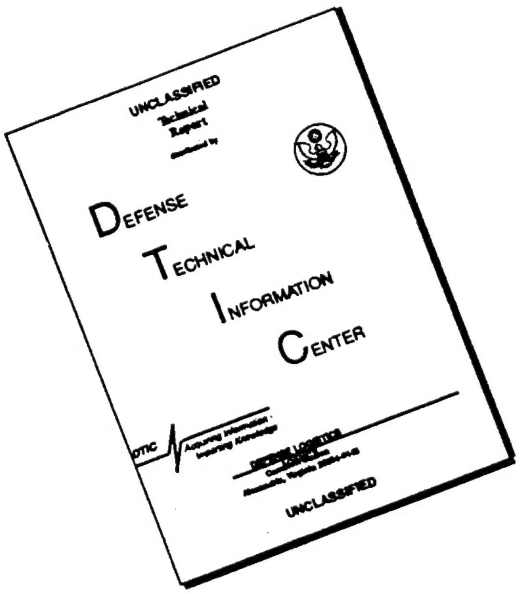

THIS DOCUMENT IS BEST QUALITY AVAILABLE. THE COPY FURNISHED TO DTIC CONTAINED A SIGNIFICANT NUMBER OF PAGES WHICH DO NOT REPRODUCE LEGIBLY.

RELATIVE PHOTOFISSION CROSS SECTIONS OF SEVERAL FISSIONABLE MATERIALS

By John McElhinney and William Ogle

ABSTRACT

The photofission excitation curve of U^{238} up to 21 Mev has been measured. An attempt has been made to determine the photofission cross-section shape as a function of energy, making appropriate assumptions as to the X-ray spectrum of the betatron. It was not possible to obtain a unique solution for the cross-section shape, but two possible solutions are given, both of which have a resonance peak at about 15 Mev.

The photofission yield of several fissionable materials relative to U^{238} has been measured in the region of the resonance. The relative yields per atom for the substances under investigation are U^{235}, 1.49; Pu^{239}, 2.51; U^{233}, 2.49; Th^{232}, 0.257; Io^{230}, 0.847; U^{238}, 1.00.

1. INTRODUCTION

The work of G. C. Baldwin and G. S. Klaiber,[1] on photofission in heavy elements aroused considerable interest in the possibility of a resonance photofission cross section.[2] After some theoretical calculation, Edward Teller suggested that the relative photofission cross sections of various fissionable materials would be of help in the theoretical interpretation of the photofission process. This work is the result of that suggestion.

A measurement of the fission yield of U^{233}, U^{235}, Pu^{249}, Th^{232}, and Io^{230}, relative to the fission yield of U^{238} has been made as a function of bremsstrahlung energy. A measurement has also been made of the photofission excitation curve of U^{238} in the region of 8 to 21 Mev. From this excitation curve an attempt has been made to determine a shape for the photofission cross section as a function of energy for U^{238}.

2. EXPERIMENTAL METHODS

The relative photofission yields of the different materials with respect to U^{238} were measured by a "catcher" method. The experimental setup is shown in Fig. 1. X rays from the betatron pass through a carbon wall 4 in. thick, into a cadmium-shielded foil holder. The carbon block was sufficiently thick to block out electrons coming directly from the betatron. The foil holder was a small aluminum box with slots in the walls at 1/8-in. spacings to hold 1/16-in. thick aluminum plates to which the fissionable material was fastened. One-mil aluminum catchers were held by small frames against the back side of the 1/16-in. alumium plates. Thus the fission fragments had to pass through 1/8 in. of air before reaching the aluminum foil. Aluminum catcher foils were used because of the small activity induced in the foil during the irradiation to which it was subjected. Eight fissionable material samples were used of which three were U^{238}. Two background aluminum foils were also in the box in order to determine the activity induced in the aluminum itself. The sample holder is shown in Fig. 2.

Two runs were made at each energy setting of the betatron, one with the beam incident on foil No. 1 and the other with the beam incident on foil No. 9. The results of these two runs were averaged

in order to minimize the effect of inverse square loss and absorption loss due to the different positions of the foils. In every case the samples were irradiated for 20 min, and counting began 4 min after the irradiation and continued for a 30-min counting interval.

The foils were counted on glass-walled counter tubes, Model 10A, Mark I, made by the Radiation Counter Laboratories. Ten counter and scaler setups were used on each run so that the foils collecting fission fragments from any particular fissionable material were always counted on the same counter. The counters were intercalibrated by means of a radioactive arsenic sample that had about the same area as the fission foils counted. The net activity was the total number of counts in 30 min minus the counter background, minus the aluminum activity, and corrected to one counter.

The arrangement used to observe the excitation function of U^{238} is shown in Fig. 3. The physical setup of the experiment required that the beam go through 3/4 in. of wood and approximately 1 1/2 in. of aluminum before reaching the detection system itself. In order to establish equilibrium between the primary gamma rays and secondary electrons, a 4-in. thickness of carbon was inserted between the source of X rays and the detection apparatus. The detector was a flat plate ion chamber in which one surface was a thick uranium sample and the other a copper collecting plate. The uranium was in the form of a 5-mil thick disc 3 in. in diameter. The gap between the uranium and the collecting plate was 1/4 in. The chamber was filled with argon at atmospheric pressure. In order to partially cancel the pulse due to the X-ray burst, a bucking chamber was placed behind the fission chamber in the beam. The bucking chamber was connected in such a manner that the output was of the opposite sign to that on the fission chamber. No fissionable material was in the bucking chamber. The output of the bucking chamber was then mixed with the output of the fission chamber and the result amplified and passed into a gating circuit that allowed only those pulses occurring within 5 microseconds of the X-ray burst to pass through. The output of the gating circuit was then fed into a discriminator and scaler where the pulses were counted. A block diagram of this circuit is given in Fig. 4. Two 1/4-R-thimbles were placed in front of the fission chamber but enough to one side that the chamber was not shadowed by the R-thimbles. The betatron was then run at various energies and the number of fission counts per R of radiation was recorded. Since the ion chamber and R-thimbles were approximately 15 m from the betatron, the detectors received uniform intensity radiation, so that no correction for different angular spread of the beam at different energies was necessary.

The energy calibration of the betatron was based upon a measurement of the observed threshold of the $N^{14}(\gamma,n)N^{13}$ reaction. The value of this threshold was calculated from the mass data of Segré's isotope chart of July 1946 to be 10.54 Mev.

3. RESULTS

1. Relative Fission Yields. Table 1 lists the weights and sizes of the fissionable materials used. The subscripts on the U^{238} notations indicate the three different uranium samples. All samples were considered to be thin compared to the fission fragment ranges with the exception of the ionium sample. Thus, no correction was made for self-absorption of the fission fragments except in the case of the ionium foil where a 4 per cent correction was applied.

The activity per atom of the fission fragments from the various fissionable materials relative to U^{238} is given in Table 2 as a function of the peak bremsstrahlung energy for each run. In order to obtain the ratios given in Table 2, the net activity of each sample was divided by the number of atoms of fissionable material in the corresponding foil, and this number was compared with the net activity per atom obtained from the U^{238} foils. Since the activity obtained at low energies was in general small, the background and aluminum activity corrections became rather large so that the possible error on the low-energy ratios given in Table 2 is larger than at higher energies. The absence of any obvious trend with energy allows us to assume the same photofission cross-section shape with energy for all fissionable materials observed. Thus, we can assume that the ratio of the activity from a fissionable substance to the activity obtained from U^{238} should be a constant independent of energy. On this basis the average ratio in each case was calculated and is shown at the bottom of the Table. The error shown is the probable error of the mean assuming that the individual numbers are all measurements of the same quantity.

In order to obtain a measure of the error in the experiment three U^{238} foils were used. The ratios of activity per atom between the different foils is shown in Table 3 as a function of energy. Since this is the relative activity per atom, the ratio in all cases should be one. Thus, the variation from one is a measure of the systematic error in the experiment. The error shown on the average is the probable error of the mean as calculated from the individual values. It is seen that while the error due to statistical variations is rather small of the order of 2 or 3 per cent, the average values themselves differ from one by as much as 15 per cent. Thus, we must conclude that in any measure of the ratio of the photofission yield, one fissionable material with relation to U^{238}, there may be a systematic error as large as 10 or 15 per cent.

B. Photofission Excitation Curve. The results of the measurement of the photofission excitation curve in U^{238} as measured with a fission ion chamber are given in Tables 4 and 5 and in Fig. 5. Table 4 lists the energy settings at which the betatron was run and the number of fissions per R observed at that energy where the number of fissions per R may be the average of several runs. In particular the data was taken starting at 19.8 Mev and running down to 8.75 Mev and repeating the points again on the way back up to 19.8 Mev. Then in order to obtain the shape of the curve at high energies in a more precise fashion the ratio of 18.9 to 20.8 Mev, the ratio of 20.8 to 21.2 Mev, and the ratio 20.8 to 21.7 Mev were obtained with greater precision by repeating these points many times. The errors quoted in Table 4 represent the variation from the mean in the several runs at each point. These data are plotted on Fig. 5 and are shown as diamonds where the vertical distance between the points of the diamond represent the probable error on the points. The values in Table 5 were taken from Fig. 5 for the purposes of calculation. The errors quoted in Table 5 are intended to represent the possible variation of the values at each point. The values in Table 5 were then used for all further calculations.

In order to calculate the shape of the photofission cross section as a function of gamma-ray energy from these data, it is necessary to know the relative number of quanta in each energy interval striking the uranium foil for each R recorded by the R-thimble. The initial X-ray spectrum emerging from the target was corrected for all absorbing materials between the target and the uranium foil. The response of the R-thimble was calculated assuming that it responded only to the secondary electrons coming out of the carbon, which were in equilibrium with the primary gamma rays. From these two calculations the number of gamma rays hitting the uranium per R was calculated. Using this number and various assumed photofission cross-section shapes an attempt was made to fit the observed excitation curve.

The calculation of the gamma-ray spectrum seen by the fission chamber and seen by the R-thimbles is given in Appendix I and the calculation of the R-thimble response is given in Appendix II.

In principle, if one knows the photofission excitation curve exactly and the gamma-ray spectrum exactly, one can arrive at a unique solution for the photofission cross section as a function of energy. However, comparatively small errors in the excitation curve lead to very large errors in the deduced cross-section curve; sufficiently large errors, in fact, that one quite soon obtains large negative values for the cross section at certain energies in order to fit the observed excitation curve. Thus, a more sensible procedure for arriving at the cross-section curve seems to be to assume various cross-section shapes and try to fit these to the excitation curve by making appropriate changes in the initially assumed cross-section curve. An effort to arrive at a cross-section curve that would fit the observed excitation curve by means of various step functions whose corners were rounded off resulted in the cross-section curve given by Sigma 2 in Table 6, which is shown plotted in Fig. 6. It did not appear possible to fit the observed curve without some sort of a resonance peak as shown in that curve. The fact that a resonance is indicated agrees with the work of Baldwin and Klaiber[1] and the theoretical considerations of Teller and Goldhaber.[2] On the assumption that a resonance cross-section curve is necessary, an attempt was made to obtain a cross-section curve of the form:

$$\sigma = \frac{A}{B + (E - E_0)^2}$$

which would fit the observed data. It was found necessary, in order to make a proper fit, effectively to cut off the curve at 9 Mev but to allow a small value at 8 Mev and no value to the cross section from there on down. Even on this basis it was found that the fit was quite critical to the parameters of the cross-section equation. The final equation obtained which gave an excitation curve that fell within the errors of Table 5 is

$$\sigma = \frac{771.88}{15.625 + (E-15)^2}$$

where E is the energy in Mev. The fact that the numbers in the above equation are given to five significant figures does not imply that we know the cross-section shape that well. These are just numbers that will give a fit to the excitation curve. It appears that with this type of resonance equation, it would be rather difficult to get a fit using a resonance peak at more than 1/2 or 1 Mev different from the 15 Mev assumed. A graph of this curve is shown in Fig. 6 and the exact values used are given in Table 6, listed under Sigma 1.

4. DISCUSSION

It is to be noted that the ratio of the ionium activity to U^{238} activity given in Table 2 has an appreciably larger error than that quoted on any of the other ratios. The main reason for this large error is that the ionium was not pure but was only 25 per cent by weight of a sample containing mostly thorium. Thus the prorated thorium activity for each point had to be subtracted from the total activity in order to obtain numbers proportional to the ionium activity. Thus any errors in the thorium curve were multiplied in the ionium curve.

It is also to be noted that we obtain a ratio for the thorium to uranium activity of approximately 1/4, whereas Baldwin and Klaiber[1] observed a ratio of 1/2. It appears that part of this discrepancy is due to the fact that Baldwin and Klaiber's fissionable material foils were all assumed to be completely thick compared with the fission fragment range. However, from the numbers that they quote it appears that their uranium sample was not completely thick. This difference might change their ratio to approximately 1 to 3, which would still leave a discrepancy between the two observed values.

It should be emphasized that the experimental excitation curve arrived at in this work does not and cannot lead to a unique photofission cross-section curve with energy. However, the data obtained here should be sufficiently good to serve as a check on a theoretically derived cross-section shape.

No correction has been applied to any of the data for possible effects of neutrons coming from the betatron. Several rough experiments were performed to determine whether this effect was appreciable or not.

The samples were irradiated in front of the betatron and then behind the betatron along with copper and rhodium foils. The 10-min period resulting from the Cu^{63} (γ,n) reaction is a measure of the gamma intensity whereas the 44-sec and 4.2-min Rh activities are a measure of the slow-neutron flux. The activity on the catchers was negligible (approximately 3 to 4 counts per min) when irradiated behind the betatron compared with several hundred counts per minute on each foil when placed in the X-ray beam. This ratio is closer to the observed copper ratio of approximately 400 than to the rhodium ratio of approximately 3.0. So one can conclude that the great majority of fissions in this experiment are produced by gamma radiation.

A cadmium shield was used around the fission foil container to reduce any effect from slow neutrons. However, when this cadmium foil was removed the observed activity did not increase more than the probable error on the measurement. The ratio of the number of fissions observed in front and behind a 2-in. thick wall of lead followed approximately the corresponding ratio for the number of gamma rays, which again makes it appear that the great proportion of the fissions observed were due to gamma rays and not neutrons. A similar experiment indicated that the great proportion of the R-thimble response was also due to gamma rays.

Appendix 1 — Bremsstrahlung Spectrum Impingent on U^{238} in the Fission Chamber

L. I. Schiff and P. Stehle[3] have derived the following formula for the differential cross-section for production of a photon in the energy interval dk and in the solid angle $dw = \sin\theta \; d\theta \; d\phi$ by the bremsstrahlung process from an electron (total energy E_0) impinging on a thin target of atomic number Z.

$$d\phi = \frac{8 Z^2 e^4 \, dw}{2\pi \times 137 \, u^4 \left[1 + \frac{(E_0 \theta)^2}{u}\right]^2} \cdot \left(\frac{E_0^2 \Gamma}{k}\right) dk$$

where

$\Gamma = 2(1-\epsilon)(L_n \alpha - 1) + \epsilon^2 (L_n \alpha - 1/2)$

E_0 = total electron energy = rest energy plus kinetic energy

$k = h\nu$

$u = m_0 c^2$

$\epsilon = k/E_0$

$$1/\alpha^2 = \left[\frac{u\epsilon}{2 E_0 (1-\epsilon)}\right]^2 + \left[\frac{Z^{1/3}}{191}\right]^2$$

Values of $(E_0^2 \Gamma)/k$ calculated from the above formula, using Z = 78 for the platinum target in the betatron and using integer values of E_0 and k, are given in Table I-A. The values within 1 Mev of either end of the spectrum are only approximations since the Born approximation used in the derivation of the above formula is not valid in these regions.

Since the target in the betatron is not infinitely thin to the passage of electrons, an approximate correction to the spectrum is desirable. From measurements of the angular spread of the X-ray beam from the betatron[4] and calculations of the theoretical spread due to multiple scattering of the electrons in the target[3,5] the effective thickness of the target is estimated to be about 1.5 Mev. An approximate thick target spectrum could be obtained by integrating the spectra formed as the primary electrons lost energy from E_0 to $(E_0 - 1.5)$ Mev over the target thickness. To do this numerically, it was assumed that no great error would be introduced if, instead of integrating, we added the appropriate weighted values of the spectra at E_0 and $(E_0 - 1)$ Mev.

To obtain these weighted values we assume that any electron passing through the betatron target in the energy range of E to E−1.5 has an equal probability of producing a photon, and that there are equal numbers of electrons of all energies in this interval. Then the resultant spectrum is the sum of the spectra resulting from every energy in this range, thus

$$S = \sum \frac{1}{2n} S_E + \frac{1}{n} S\left[E - \frac{1.5}{n}\right] \frac{1}{n} S\left[E - \frac{2(1.5)}{n}\right] \cdots \frac{1}{2n} S\left[E - \frac{n(1.5)}{n}\right]$$

where S is the resultant spectrum, S_E is the spectrum due to electrons of energy E, and n is the number of intervals into which we divide the 1.5-Mev interval. The first and last terms are divided by two in order to weight the end points only half as much as the rest. If we now set n equal to three we get

$$S = \frac{1}{6} \sum S_E + 2 S_{(E-.5)} + 2 S_{(E-1)} + S_{(E-1.5)}$$

If we now assume that

$$\frac{S_E + S_{(E-1)}}{2} = S_{(E-.5)}$$

and

$$S_{(E-.5)} + S_{(E-1.5)} = 2\,S_{(E-1)}$$

we get

$$S = \frac{1}{4}\sum S_E + 3\,S_{(E-1)}$$

Thus we add three times the thin target spectrum at E−1 to the thin target spectrum at E to obtain the new thick target spectrum at E. The result of this is given in Table I-B.

In order to obtain the spectrum incident on the uranium in the ion chamber, the absorption coefficients for the Compton effect and the pair production of integer energies up to 21 Mev for the various absorbing materials between the target and the uranium were calculated.[6] Absorption due to the photoelectric effect was negligible at these energies. The absorption coefficients (τ) times the material thicknesses (x) are listed in Table I-C and the final transmission as a function of energy is listed in the last column. The spectra impinging on the uranium are obtained by multiplying the thick target spectra by the transmission coefficients. Table I-D tabulates these spectra after being normalized as described in Appendix 2. Since the ion chamber is far enough from the betatron that it receives a practically uniform radiation, the conversion from photons per unit solid angle to photons per cm² can be made by a constant factor that does not change the shape of the spectra.

Appendix 2—R-Thimble Response

The betatron X rays were monitored with two 1/4-R-thimbles in the beam. In order to get a measure of the number of quanta striking the uranium per R recorded in the R-thimble, it is necessary to know the R-thimble response to different energy quanta.

Consider a thick wall of carbon (i.e., thick compared with the range of the secondary electrons) placed in front of the R-thimble. Associated with each emerging quantum will be a certain number of electrons and positrons formed by the Compton process and pair production. $R_c(k)$ represents the average forward component of the range of Compton electrons from a quantum of energy k, and $R_p(k)$ represents the average forward component of the positrons and electrons from pair production by a quantum of energy k.

For simplicity we assumed that all electrons and positrons emerging from the carbon form an average ionization of 60 ion pairs per centimeter in air regardless of their energy. And we also assumed that the R-thimble has no response to gamma rays themselves but only to the secondary electrons and positrons.

The average number of Compton electrons emerging from the carbon per emerging photon of energy k is $(e^{\tau R_c}-1)\tau_c/\tau$, and the average number of particles from pair production emerging from the carbon per emerging photon of energy k is $2\,(e^{\tau R_p}-1)\tau_p/\tau$, where τ_c = absorption coefficient of gammas in carbon due to the Compton process, τ_p = absorption coefficient of gammas in carbon due to pair production, and $\tau = \tau_c + \tau_p$. (τ, τ_c, τ_p, R_c, and R_p are all functions of k.)

The number of R behind the carbon per emerging quantum of energy k per square centimeter is therefore

$$T = 4.8\times 10^{-10}\ \frac{\text{esu}}{\text{ion}} \times 60\ \frac{\text{ions}}{\text{cm}} \left[(e^{\tau R_c}-1)\frac{\tau_c}{\tau} + 2(e^{\tau R_p}-1)\frac{\tau_p}{\tau}\right] \frac{\text{elec/cm}^2}{\text{quanta/cm}^2}$$

$$T = 2.88\times 10^{-8} \left[(e^{\tau R_c}-1)\frac{\tau_c}{\tau} + 2(e^{\tau R_p}-1)\frac{\tau_p}{\tau}\right] \frac{\text{R}}{\text{quanta/cm}^2}$$

The values of R_C were estimated from the results of the calculated average at 1, 10, and 20 Mev. (This calculation was based on formula 52, p. 156 in Heitler[6] in combination with energy and momentum conservation equations. The number and energy of Compton electrons at each angle were calculated and the average forward component of the range was obtained.) The range in gm/cm^2 was assumed to be the same in carbon as aluminum. Values of R_C are shown in Table II-A.

The values of R_p were obtained by taking the range of an electron (or positron) of energy $\frac{k-1}{2}$ and multiplying it by an estimated factor to obtain the average forward component. This estimated factor varied from 0.5 at low energies to 1.0 above 10 Mev. Again the range of the secondary electrons (and positrons) were assumed to be the same in gm/cm^2 of carbon as in aluminum. Values are shown in Table II-A.

The absorption coefficients, τ_c and τ_p, for carbon were calculated from formulae given by Heitler[6] and are listed in Table II-A. Substituting these values in the above formula for T, the response shown in the last column is obtained. A plot of the R-thimble response is shown in Fig. II-A. It is approximately proportional to the energy.

In order to determine the magnitude of the spectra striking the uranium when the R-thimble totals 1 R, it is necessary to calculate the spectra which strike the R-thimble. These are readily obtained using the thick target spectra tabulated in Table I-B and the transmission coefficients up to the R-thimble tabulated in Table I-C. These spectra are multiplied by the R-thimble response and integrated over all k for a given E_0. The final sum is the necessary normalization factor and is divided into the spectra incident on the uranium to obtain the normalized spectra per R listed in Table I-D.

A point at $E_0 - m_0c^2$ on the excitation function is the sum over all k of the products of the cross section and the normalized spectrum for E_0.

REFERENCES

1. G. C. Baldwin and G. S. Klaiber, Phys. Rev., 71: 3 (1947).
2. M. Goldhaber and E. Teller, Phys. Rev., 74: 1046 (1948).
3. L. I. Schiff and P. Stehle, LA Report No. 375.
4. J. McElhinney, Thesis, University of Illinois (1947).
5. L. I. Schiff, Phys. Rev., 70: 89 (1946).
6. W. Heitler, "The Quantum Theory of Radiation," pp. 157, 200, Oxford University Press, New York, 1944.

Table 1

Sample	Weight	Area	gm/cm²
U^{238}_{I}	0.002536 gm	23.5 cm²	1.08×10^{-4}
U^{238}_{II}	0.002356 gm	24.0 cm²	0.982×10^{-4}
U^{238}_{III}	0.002485 gm	24.5 cm²	1.014×10^{-4}
Pu^{239}	0.001367 gm	13.8 cm²	0.9906×10^{-4}
Io^{230} *	(0.001042 gm	11.9 cm²	0.8756×10^{-4}
Th^{232} *	(0.003276 gm		2.7530×10^{-4}
$Th^{232}O_2$	0.00290 gm = 0.00255 gm Th	24.3 cm²	1.049×10^{-4}
$(U^{235})_3O_8$	0.00307 gm = 0.00261 gm U^{235}	27.3 cm²	0.956×10^{-4}

*These weights derived from the original data of a total alpha decay rate of 45,687,000 per minute in 100 per cent geometry and 25 per cent ionium by weight.

Table 2—Relative Activity Per Atom

Energy	U^{235}/U^{238}	Pu^{239}/U^{238}	U^{233}/U^{238}	Th^{232}/U^{238}	Io^{230}/U^{238}
12.4 Mev	1.45	2.70	3.26	0.218	1.645
14.3	1.59	2.74	2.87	0.247	0.836
16.1	1.59	2.54	2.68	0.276	0.907
17.1	1.44	2.24	3.01	0.352	0.466
18.0	1.57	2.70	2.22	0.254	0.783
18.9	1.47	2.60	2.06	0.260	0.672
19.8	1.43	2.39	2.13	0.209	0.894
20.8	1.31	2.06	1.90	0.227	0.602
21.7	1.54	2.65	2.29	0.273	0.816
Average	1.49±0.02*	2.51±0.05*	2.49±0.11*	0.257±0.010*	0.847±0.075*

*This error is the probable error of the mean assuming that the individual numbers are all measurements of the same quantity. As seen from Table 3 there may be an additional systematic error as great as 15 per cent.

Table 3—Uranium Activity Comparison

Energy, Mev	U_I^{238}/U_{II}^{238}*	$U_{II}^{238}/U_{III}^{238}$*	U_{III}^{238}/U_I^{238}*
12.4	1.30	1.15	0.671
14.3	1.20	1.12	0.741
16.1	1.09	1.12	0.818
17.1	1.03	0.995	0.976
18.00	1.13	1.04	0.856
18.9	1.00	0.998	1.001
19.8	1.11	1.04	0.866
20.8	1.23	0.867	0.937
21.7	1.00	1.28	0.784
Average	1.12±0.02	1.07±0.03	0.850±0.025

*The subscripts I, II, and III indicate the different uranium foils.

Table 4

Energy	Counts/R
8.75	42 ± 42
10.59	883 ± 32
12.4	1726 ± 75
14.3	3010 ± 37
16.1	4372 ± 69
17.1	4756 ± 150
18.0	4918 ± 55
18.9	5443 ± 78
19.8	5434 ± 148
20.8	5971 ± 157
21.2	5663 ± 182
21.7	5995 ± 163

Table 5

Energy	Counts/R
7.5	0
8.5	0 ± 60
9.5	320 ± 60
10.5	790 ± 70
11.5	1280 ± 100
12.5	1840 ± 100
13.5	2420 ± 100
14.5	3120 ± 100
15.5	3880 ± 100
16.5	4480 ± 120
17.5	4900 ± 150
18.5	5220 ± 170
19.5	5480 ± 200
20.5	5720 ± 220
21.5	5920 ± 220

Table 6—Possible Cross-Section Curves*

Energy	$Sigma_1$	$Sigma_2$
0 to 7	0	0
8	6.690	6.00
9	14.95	17.40
10	19.00	19.40
11	24.40	21.2
12	31.34	23.2
13	39.34	54.0
14	46.42	59.0
15	49.40	30.8
16	46.42	31.0
17	39.34	32.8
18	31.34	34.8
19	24.40	36.8
20	19.00	38.6
21	14.95	40.6

*Where $\sigma_1 = \frac{771.88}{15.625 + (E-15)^2}$ down to 9 Mev.

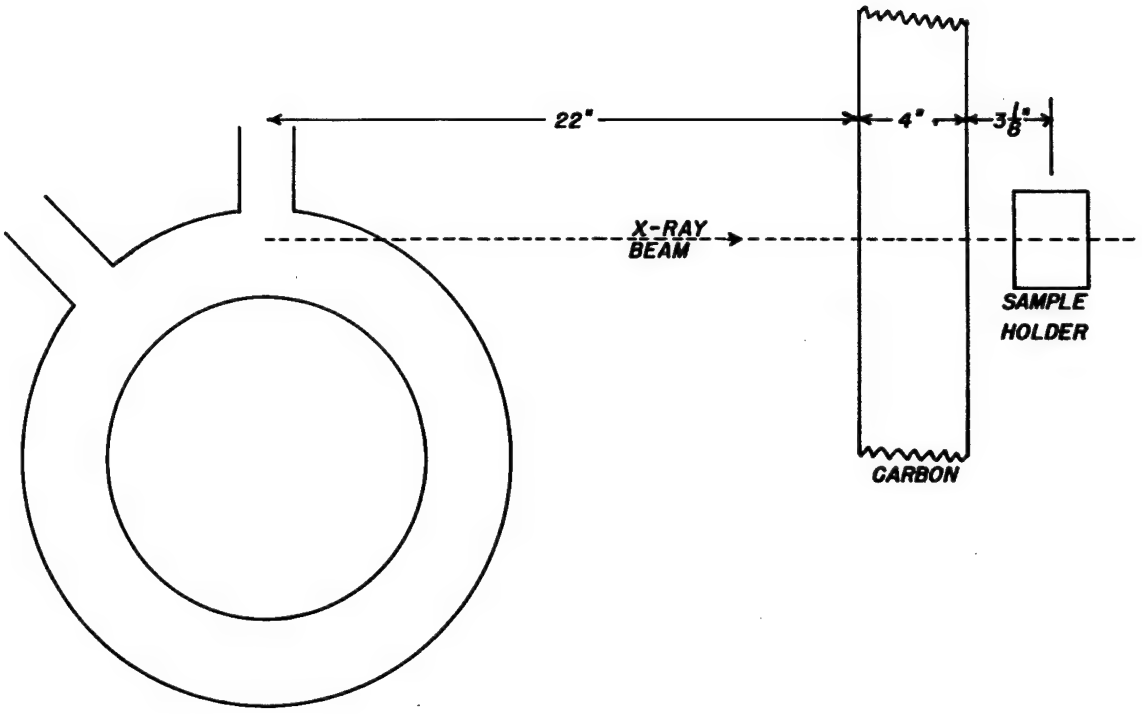

Fig. 1—Irradiation geometry for relative photofission yields.

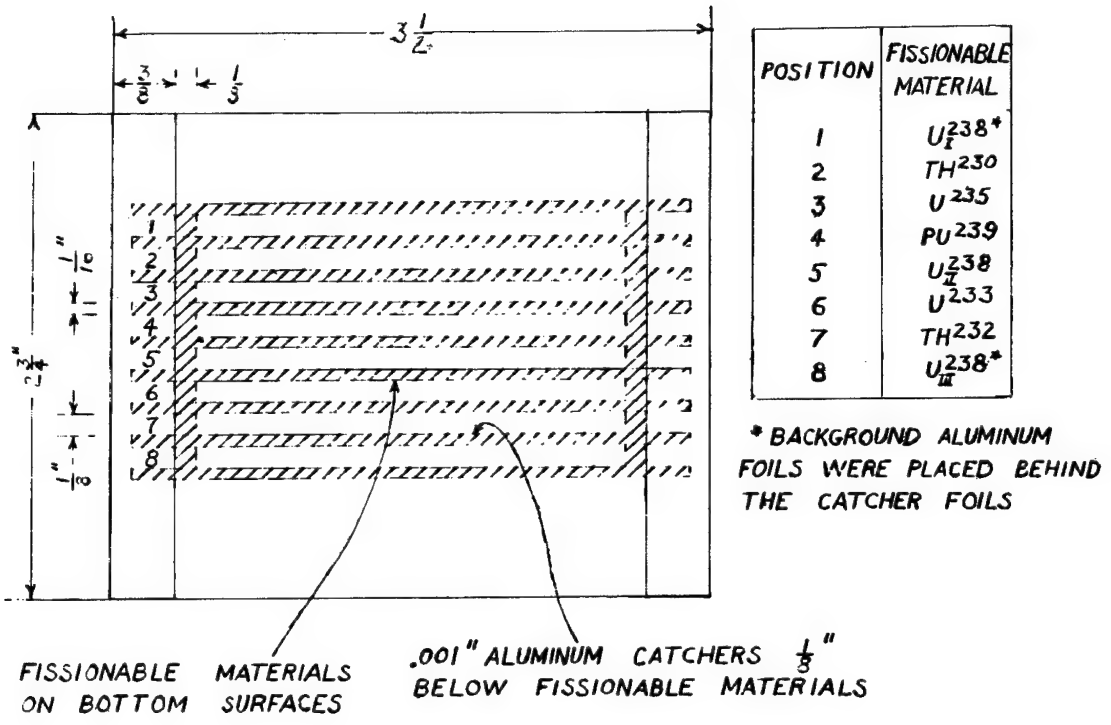

POSITION	FISSIONABLE MATERIAL
1	U_{I}^{238}*
2	TH^{230}
3	U^{235}
4	PU^{239}
5	U_{II}^{238}
6	U^{233}
7	TH^{232}
8	U_{III}^{238}*

* BACKGROUND ALUMINUM FOILS WERE PLACED BEHIND THE CATCHER FOILS

Fig. 2 — Sample holder.

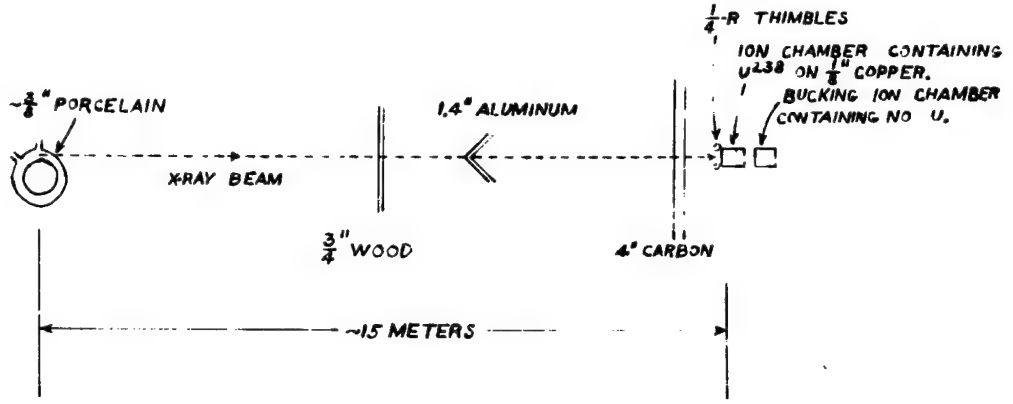

Fig. 3—Irradiation geometry for excitation function.

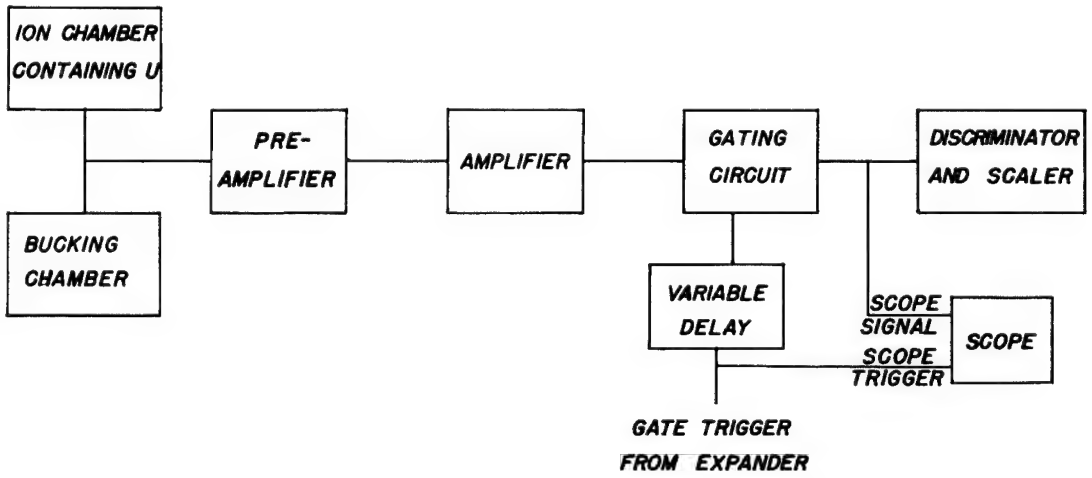

Fig. 4—Circuit arrangement for observing fission pulses.

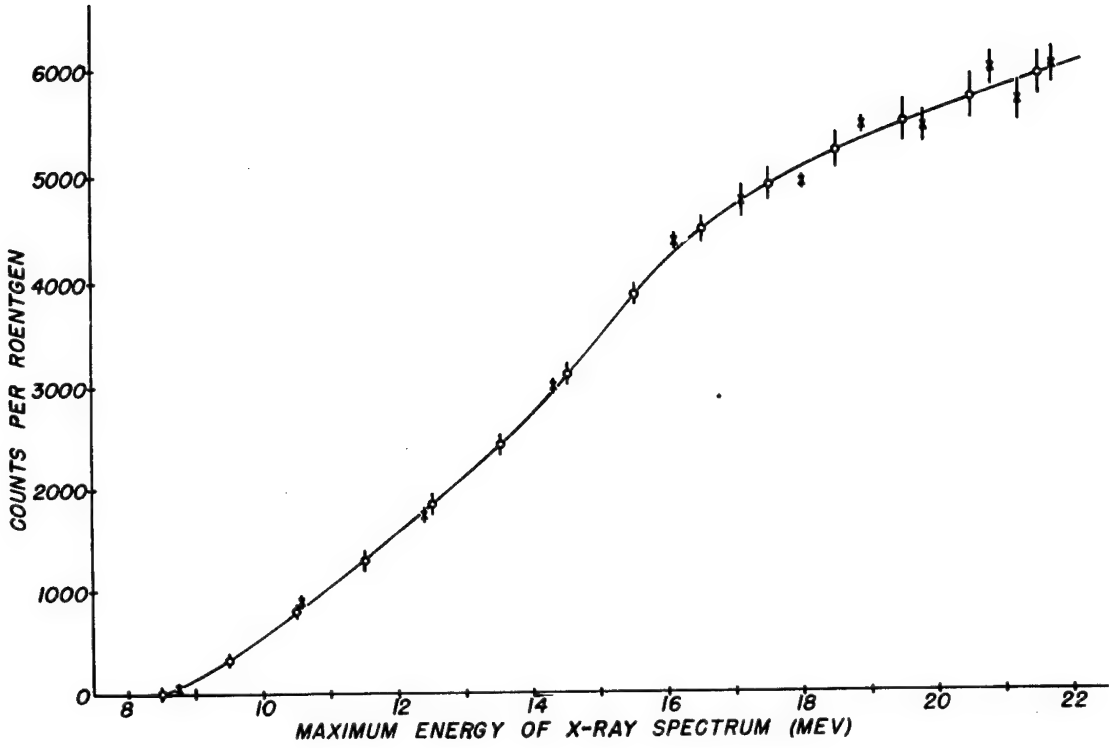

Fig. 5 — Excitation function for $U^{238}(\gamma,f)$.

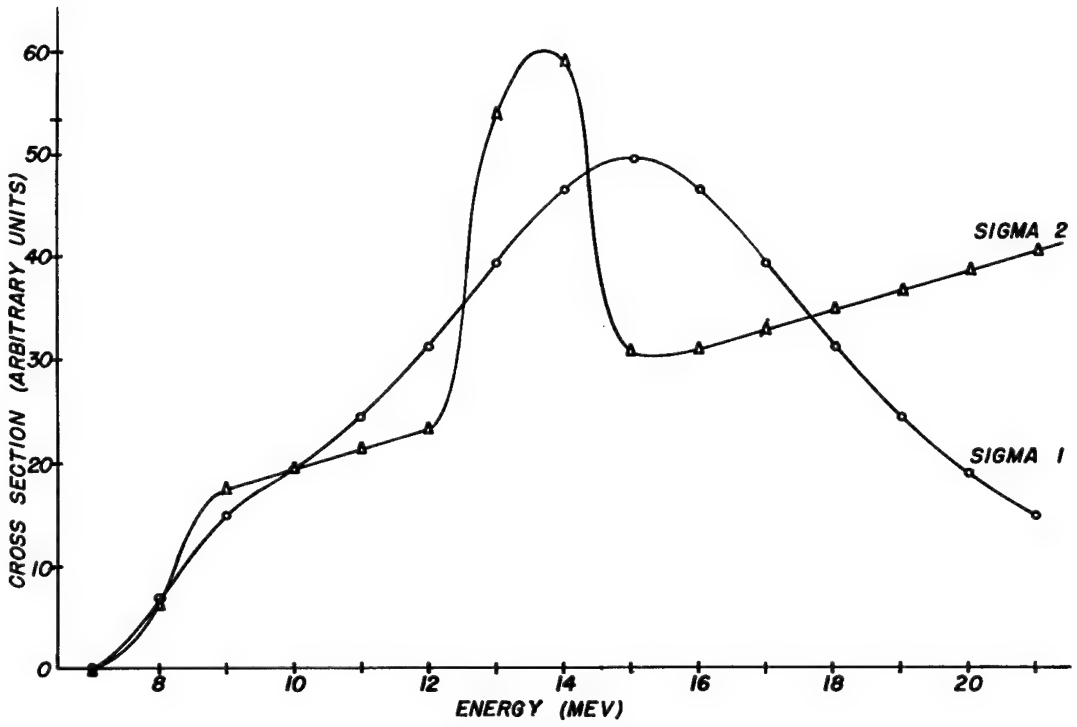

Fig. 6 — Possible (γ,f) cross section shapes.

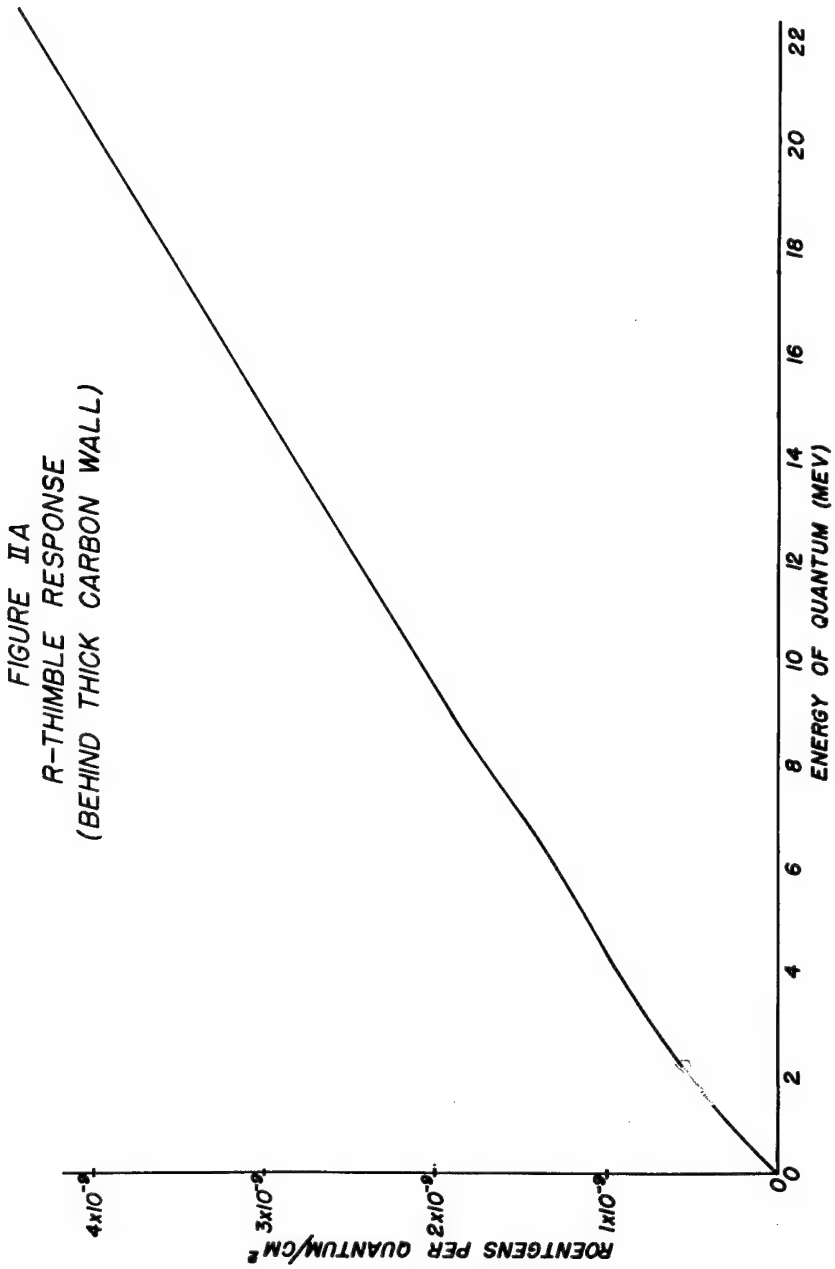

Fig. IIA — R-thimble response (behind thick carbon wall).

Table I-A

$E_0^2 \frac{\Gamma}{k}$: Proportional to $\frac{\text{Photons/unit solid angle/Mev}}{\text{electron}}$ for thin target (straight forward).

E_0 / k	6	7	8	9	10	11	12	13	14	15	16	17	18	19	20	21	22	Mev
0	∞	∞	∞	∞	∞	∞	∞	∞	∞	∞	∞	∞	∞	∞	∞	∞	∞	
1	167	236	315	405	505	619	743	877	1023	1177	1347	1520	1717	1917	2132	2355	2589	
2	65.5	98.0	136	179	228	282	340	406	474	551	635	722	813	910	1016	1125	1239	
3	32.0	52.4	76.8	104	135	169	207	250	296	344	397	454	512	578	644	714	789	
4	16.3	30.0	46.9	66.9	89.2	115	143	172	206	241	279	321	366	412	460	512	566	
5	6.52	17.0	29.5	44.6	62.0	81.8	103	127	153	180	210	242	276	312	350	392	434	
6	0	7.3	18.0	30.0	44.0	59.7	77.3	96.8	117	140	164	191	218	247	278	312	345	
7	0	0	8.13	19.1	30.7	44.6	58.9	74.9	93.9	112	132	153	177	201	228	256	284	
8	0	0	0	8.91	20.4	31.9	44.6	58.5	73.9	90.2	108	127	147	168	190	213	239	
9	0	0	0	0	9.72	21.8	33.3	46.1	59.2	73.6	89.3	106	124	141	161	181	203	
10	0	0	0	0	0	10.6	23.0	34.6	46.8	60.8	74.0	88.7	104	121	138	156	175	
11	0	0	0	0	0	0	11.4	24.5	36.3	48.4	61.2	74.6	89.1	104	119	136	153	
12	0	0	0	0	0	0	0	12.4	26.1	38.0	49.9	62.4	75.5	89.5	104	119	134	
13	0	0	0	0	0	0	0	0	13.2	27.2	39.7	51.4	63.8	76.9	90.4	104	119	
14	0	0	0	0	0	0	0	0	0	14.1	28.7	41.3	53.8	66.1	78.4	91.3	105	
15	0	0	0	0	0	0	0	0	0	0	14.7	30.6	43.7	55.2	67.6	79.8	92.9	
16	0	0	0	0	0	0	0	0	0	0	0	15.8	31.8	44.8	57.2	69.2	80.3	
17	0	0	0	0	0	0	0	0	0	0	0	0	16.6	33.4	46.8	59.1	70.7	
18	0	0	0	0	0	0	0	0	0	0	0	0	0	17.5	34.7	48.5	61.0	
19	0	0	0	0	0	0	0	0	0	0	0	0	0	0	18.2	36.2	50.3	
20	0	0	0	0	0	0	0	0	0	0	0	0	0	0	0	19.1	39.9	
21	0	0	0	0	0	0	0	0	0	0	0	0	0	0	0	0	19.9	

Mev

Table I-B

Values of $\frac{1}{k}\left[3(E_0-1)^2\,\Gamma\,(E_0-1) + E_0^2\,\Gamma\,(E_0)\right]$. Approximate thick target spectrum proportional to $\frac{\text{Photons/unit solid angle/Mev}}{\text{electrons}}$ (straight forward).

E_0 / k	7	8	9	10	11	12	13	14	15	16	17	18	19	20	21	22	Mev
1	737	1023	1350	1720	2134	2600	3106	3654	4246	4878	5561	6277	7068	7883	8751	9654	
2	294	430	587	765	966	1186	1426	1692	1973	2288	2627	2979	3349	3746	4173	4614	
3	148	234	335	447	574	714	871	1046	1232	1429	1645	1874	2114	2378	2646	2931	
4	78.9	137	208	290	382	488	601	722	859	1002	1158	1329	1510	1696	1892	2102	
5	36.5	80.5	134	196	268	349	436	534	639	750	872	1002	1140	1286	1442	1610	
6	7.30	39.9	84.0	134	192	257	329	407	491	584	683	791	901	1019	1146	1281	
7	0	8.13	43.5	88	137	193	252	319	394	468	549	636	732	831	940	1052	
8	0	0	8.91	47.1	93.1	140	192	249	312	379	451	528	609	694	783	878	
9	0	0	0	9.72	51.0	98.7	146	198	251	310	374	442	513	584	664	746	
10	0	0	0	0	10.6	54.8	104	151	201	256	311	370	433	501	570	643	
11	0	0	0	0	0	11.4	58.7	110	157	206	258	313	371	431	493	561	
12	0	0	0	0	0	0	12.4	63.3	116	164	212	263	316	373	431	491	
13	0	0	0	0	0	0	0	13.2	66.8	121	171	218	268	321	375	431	
14	0	0	0	0	0	0	0	0	14.1	71.0	127	178	228	277	327	379	
15	0	0	0	0	0	0	0	0	0	14.7	74.7	136	186	233	283	332	
16	0	0	0	0	0	0	0	0	0	0	15.8	79.2	140	192	241	288	
17	0	0	0	0	0	0	0	0	0	0	0	16.6	83.2	147	200	248	
18	0	0	0	0	0	0	0	0	0	0	0	0	17.5	87.2	153	207	
19	0	0	0	0	0	0	0	0	0	0	0	0	0	18.2	90.8	159	
20	0	0	0	0	0	0	0	0	0	0	0	0	0	0	19.1	97.2	
21	0	0	0	0	0	0	0	0	0	0	0	0	0	0	0	19.9	
Mev																	

Table I-C

Transmission coefficients.

k	A Donut τx	B 3/4" Wood τx	C 1.4" Alum. τx	D .4" Carbon τx	E 1/8" Copper τx	$(\tau x)_o$ A + B + C + D	Transmission to R-thimble $e^{-(\tau x)_o}$	$(\tau x)_{total}$ A + B + C + D + E	Transmission up to U in fission chamber $e^{-(\tau x)_{total}}$
1	.1862	.0767	.592	1.025	.162	1.880	.1526	2.042	.1298
2	.1309	.0535	.416	.708	.117	1.308	.2704	1.425	.2405
3	.1065	.0429	.340	.572	.100	1.061	.3461	1.161	.3132
4	.0923	.0367	.299	.494	.0927	.922	.3977	1.015	.3624
5	.0831	.0325	.271	.437	.0883	.824	.4387	.912	.4017
6	.0775	.0298	.255	.396	.0873	.758	.4686	.845	.4296
7	.0732	.0276	.243	.368	.0867	.712	.4907	.799	.4498
8	.0698	.0259	.233	.344	.0867	.673	.5102	.760	.4677
9	.0674	.0246	.227	.326	.0873	.645	.5247	.732	.4809
10	.0653	.0234	.221	.311	.0876	.621	.5374	.709	.4921
11	.0637	.0226	.217	.298	.0883	.601	.5483	.689	.5021
12	.0623	.0218	.214	.288	.0892	.586	.5565	.675	.5092
13	.0613	.0212	.211	.279	.0899	.572	.5644	.662	.5158
14	.0605	.0206	.210	.272	.0911	.563	.5695	.654	.5200
15	.0597	.0202	.208	.265	.0921	.553	.5752	.645	.5247
16	.0591	.0198	.206	.259	.0930	.544	.5804	.637	.5289
17	.0587	.0194	.206	.255	.0940	.539	.5833	.633	.5310
18	.0582	.0191	.205	.250	.0953	.532	.5874	.627	.5342
19	.0580	.0188	.205	.246	.0962	.528	.5898	.624	.5358
20	.0578	.0186	.205	.243	.0972	.524	.5921	.621	.5374
21	.0576	.0184	.205	.240	.0984	.521	.5939	.619	.5385
22	.0574	.0182	.205	.237	.0994	.518	.5957	.617	.5396

Mev

Table I-D

$$\text{Numbers above} = \frac{\text{Quanta/cm}^2}{\text{R} \times \text{Mev interval}}$$

Normalized spectra - photons per cm^2 per Mev interval incident on uranium per Roentgen recorded in R-thimbles.

E_o / k	7	8	9	10	11	12	13	14	15	16	17	18	19	20	21	22	Mev
1	571.7	455.9	374.3	315.9	271.1	237.1	210.3	187.6	169.6	154.4	141.7	130.5	121.6	113.4	106.4	100.0	
2	422.3	355.0	301.6	260.3	227.4	200.4	178.9	161.0	146.0	134.2	124.0	114.8	106.7	99.9	94.0	88.6	
3	277.2	251.6	224.1	198.0	176.0	157.1	142.3	129.6	118.7	109.2	101.1	94.0	87.7	82.6	77.6	73.3	
4	170.8	170.3	161.1	148.7	135.5	124.3	113.6	103.5	95.8	88.5	82.4	77.1	72.5	68.1	64.2	60.8	
5	87.8	110.9	114.9	111.3	105.4	98.5	91.3	84.9	79.0	73.5	68.8	64.5	60.7	57.3	54.3	51.6	
6	18.8	58.7	77.1	81.5	80.8	77.6	73.7	69.2	64.9	61.2	57.6	54.4	51.3	48.5	46.1	43.9	
7	0	12.6	41.9	56.0	60.3	61.0	59.1	56.8	54.5	51.3	48.5	45.8	43.6	41.4	39.6	37.8	
8	0	0	8.91	31.1	42.6	46.0	46.8	46.1	44.9	43.2	41.4	39.5	37.7	36.0	34.3	32.8	
9	0	0	0	6.61	24.0	33.4	36.6	37.7	37.1	36.4	35.3	34.1	32.7	31.1	29.9	28.6	
10	0	0	0	0	5.11	19.0	26.7	29.4	30.4	30.7	30.0	29.2	28.2	27.3	26.3	25.3	
11	0	0	0	0	0	4.02	15.4	21.8	24.2	25.1	25.4	25.2	24.7	24.0	23.2	22.5	
12	0	0	0	0	0	0	3.29	12.7	18.2	20.4	21.2	21.4	21.3	21.1	20.6	20.0	
13	0	0	0	0	0	0	0	2.69	10.6	15.2	17.3	18.0	18.3	18.4	18.1	17.7	
14	0	0	0	0	0	0	0	0	2.26	9.00	13.0	14.8	15.7	16.0	15.9	15.7	
15	0	0	0	0	0	0	0	0	0	1.88	7.70	11.4	12.9	13.6	13.9	13.9	
16	0	0	0	0	0	0	0	0	0	0	1.64	6.71	9.81	11.3	11.9	12.2	
17	0	0	0	0	0	0	0	0	0	0	0	1.41	5.86	8.66	9.95	10.5	
18	0	0	0	0	0	0	0	0	0	0	0	0	1.24	5.17	7.65	8.83	
19	0	0	0	0	0	0	0	0	0	0	0	0	0	1.08	4.56	6.80	
20	0	0	0	0	0	0	0	0	0	0	0	0	0	0	.965	4.17	
21	0	0	0	0	0	0	0	0	0	0	0	0	0	0	0	.854	
Mev																	

Table II-A—R-thimble Response

Quanta energy, Mev	R_c, cm carbon	R_p, cm carbon	τ_c, 1/cm carbon	τ_p, 1/cm carbon	τ, 1/cm carbon	R Quanta/cm^2
1	0.094	0	0.1009	0	0.1009	0.27×10^{-9}
2	0.24	0.05	0.06916	0.000530	0.06969	0.54×10^{-9}
3	0.41	0.16	0.05488	0.00147	0.05635	0.76×10^{-9}
4	0.62	0.29	0.04620	0.00244	0.04864	0.94×10^{-9}
5	0.85	0.46	0.03976	0.00321	0.04297	1.09×10^{-9}
6	1.10	0.64	0.03500	0.00398	0.03898	1.28×10^{-9}
7	1.36	0.84	0.03153	0.00464	0.03617	1.48×10^{-9}
8	1.63	1.05	0.02864	0.00522	0.03386	1.72×10^{-9}
9	1.91	1.25	0.02635	0.00577	0.03212	1.93×10^{-9}
10	2.17	1.43	0.02436	0.00621	0.03057	2.09×10^{-9}
11	2.43	1.62	0.02268	0.00663	0.02931	2.29×10^{-9}
12	2.70	1.78	0.02128	0.00704	0.02832	2.47×10^{-9}
13	2.97	1.95	0.02006	0.00742	0.02748	2.66×10^{-9}
14	3.25	2.12	0.01898	0.00779	0.02677	2.83×10^{-9}
15	3.51	2.29	0.01802	0.00809	0.02611	3.02×10^{-9}
16	3.79	2.46	0.01711	0.00838	0.02549	3.20×10^{-9}
17	4.06	2.63	0.01638	0.00870	0.02508	3.37×10^{-9}
18	4.33	2.80	0.01567	0.00896	0.02463	3.57×10^{-9}
19	4.60	2.97	0.01501	0.00923	0.02424	3.74×10^{-9}
20	4.86	3.14	0.01445	0.00949	0.02394	3.95×10^{-9}
21	5.13	3.31	0.01393	0.00974	0.02367	4.12×10^{-9}
22	5.41	3.48	0.01338	0.00998	0.02336	4.32×10^{-9}

END OF DOCUMENT